Highlights

- the kinetic arrest of martensitic transformation observed in NiCoMnIn melt-spun ribbons was studied by means of magnetization measurements as a function temperature, field and time.

- the metastable character of the non-equilibrium field-cooled glassy state was characterized by introducing thermal and magnetic field fluctuations or measuring the relaxation of magnetization.

- the relationship between occurrence of exchange bias and the frozen fraction of austenite into the martensite matrix is shown.

Characterization of the kinetic arrest of martensitic transformation in $Ni_{45}Co_5Mn_{36.8}In_{13.2}$ melt-spun ribbons

F.M. Lino-Zapata[a], H.L. Yan[b,*], D. Ríos-Jara[a], J.L. Sánchez Llamazares[a,*], Y.D. Zhang[c,d], X. Zhao[b], L. Zuo[b]

[a]*Instituto Potosino de Investigación Científica y Tecnológica A.C., Camino a la Presa San José 2055 Col. Lomas 4ª sección, San Luis Potosí 78216, San Luis Potosí, México.*
[b]*Key Laboratory for Anisotropy and Texture of Materials (Ministry of Education), School of Material Science and Engineering, Northeastern University, Shenyang 110819, China.*
[c]*Laboratoire d'Étude des Microstructures et de Mécanique des Matériaux (LEM3), CNRS UMR 7239, Université de Lorraine, 57045 Metz, France.*
[d]*Laboratory of Excellence on Design of Alloy Metals for low-mAss Structures (DAMAS), Université de Lorraine, 57045 Metz, France.*

Abstract. The kinetic arrest (KA) of martensitic transformation (MT) observed in $Ni_{45}Co_5Mn_{36.8}In_{13.2}$ melt-spun ribbons has been studied. These alloy ribbons show an ordered columnar-like grain microstructure with the longer grain axis growing perpendicular to ribbon plane and transform martensitically from a single austenitic (AST) parent phase with the $L2_1$-type crystal structure to a monoclinic incommensurate 6M modulated martensite (MST). Results show that the volume fraction of austenite frozen into the martensitic matrix is proportional to the applied magnetic field. A fully arrest of the structural transition is found for a magnetic field of 7 T. The metastable character of the non-equilibrium field-cooled glassy state was characterized by introducing thermal and magnetic field fluctuations or measuring the relaxation of magnetization. The relaxation of magnetization from a field-cooled kinetically arrested state at 5 and 7 T follows the Kohlrausch–Williams–Watts (KWW) stretched exponential function with a β exponent around 0.95 indicating the weak metastable nature of the system under the strong magnetic fields. The relationship between the occurrence of exchange bias and the frozen fraction of AST into the MST matrix was studied.

Keywords Ni-Co-Mn-In shape memory alloys; melt-spun ribbons; kinetic arrest of martensitic transformation.

[*]Corresponding author. *E-mail address*: jose.sanchez@ipicyt.edu.mx (J.L. Sánchez Llamazares).
[*]Corresponding author. *E-mail address*: yanhaile@mail.neu.edu.cn (Haile Yan).

1. Introduction

The kinetic arrest (KA) of martensitic transformation (MT) is one of magnetic-field induced phenomena observed in ferromagnetic shape memory alloys of the ternary alloy systems Ni-Mn-X (X= Sn, In, Sb). It was first reported by *Sharma et al*. in a bulk $Ni_{50}Mn_{34}In_{16}$ alloy [1], and later in other Ni-rich [2-13] and Mn-rich [14-16] Heusler-type Ni-Mn-X alloys. However, this uncommon phenomenon also appears in a variety of other materials exhibiting first-order phase transitions, either alloys or oxides, such as the Laves phases $Ce(Fe,X)_2$ (X= Al, Ru) [17-20] and $HfFe_2$ [21], Gd_5Ge_4 [22], MnSi [23], NiCoMnAl [24], Mn_2PtGa [25], $Mn_3GaC_{0.9}$ [26] and phase-separated manganites [20, 27-29]. An overview about its manifestation and phenomenology in different magnetic materials can be found in Ref. 30.

In the case of Ni-rich and Mn-rich Heusler-type alloys, a fraction of the parent austenite phase will be frozen into the equilibrium martensitic matrix when the material is cooled down below the martensitic finishing structural transition temperature M_f under the effect of a static magnetic field of strength beyond a certain critical value. The supercooled austenite phase experiences a viscous retardation of nucleation and growth, giving rise to a nonergodic glasslike state [19]. At present, it is still a great challenge to fully understand the nature of this kind of glass transitions [31, 32], and the correlated KA effect is considered as one of the deepest and most important unsolved problems in condensed matter physics [33].

This mixed, or two-phase, state is metastable in nature and is commonly characterized by means of magnetization measurements [1, 2, 4, 19]; however, in some cases the biphasic state has been also studied through the temperature dependence of dc electrical resistivity [2, 30], Hall probe imaging [18] and neutron diffraction measurements [16]. The relevant information provided by these experiments is found when one compare the information obtained from the zero-field-cooled (ZFC) and field-cooled (FC) states in the phase coexistence region (i.e., in the existence temperature region of martensite). As expected, due to the higher saturation

magnetization of austenite (AST) with respect to martensite (MST), the zero-field cooling and field-cooling and field-heating (FH) pathways of the temperature dependence of magnetization $\sigma(T)$ split in the martensite existence region [1-16].

The temperature influence on KA effect in these alloys has been related to the extremely low mobility of the phase interfaces (habit plane) and an abnormal behavior in transformation entropy change at low temperatures [2, 4]. However, the underlying mechanism of the KA effect in these Ni-Mn-X based alloys is still unclear. As in origin the KA effect means the incompleteness of martensitic transformation, it should has a close connection with the local crystallographic and stress-strain relationships between the parent and product phases through the martensitic transformation under the presence of the applied magnetic field. Thus, the influence of magnetic and temperature field on materials parameters associated to the MT such as lattice parameters and elastic modulus should provide useful knowledge to deeply understand this effect.

Most of the studies carried out on the observation and characterization of the KA phenomenon in Ni-rich and Mn-rich Heusler-type alloys have been performed in bulk alloys. In the case of melt-spun ribbons, the field-induced arrest of MT has been only reported in a few alloys such as $Mn_{50}Ni_{40}In_{10}$ [14], $Ni_{52.2}Mn_{34.3}In_{13.5}$ [13], $Ni_{45}Co_5Mn_{38}Sn_{12}$ [10], $Ni_{38}Co_{12}Mn_{41}Sn_9$ [11], and $Ni_{47}Mn_{35}Fe_5In_{13}$ [12]. However, most of these studies are limited to report its existence based on the above mentioned splitting between ZFC and FC(FH) $\sigma(T)$ curves, whereas no further characterization is presented. For the investigation of this phenomenon melt-spun ribbons present two important advantages. First, they show a much more homogeneous chemical composition in comparison with bulk alloys since the molten alloy is rapidly solidified during ribbon formation. Second, a proper control of synthesis parameters may produce a microstructure formed by columnar in shape highly oriented grains growing through the entire ribbon thickness (as occurs for the ribbon samples here studied). Hence, the applied magnetic field direction, that is usually along ribbon length, keeps constant with respect to the preferred crystal growth direction

facilitating any analysis of crystallographic preferred orientation of ribbon.

In this manuscript, we present an experimental study the kinetic arrest of MT in $Ni_{45}Co_5Mn_{36.8}In_{13.2}$ melt-spun ribbons by means of different magnetization measurements (as a function temperature, field and time). After a comprehensive structural, microstructural and thermomagnetic characterization of samples, emphasis is given to characterize the metastable character of the kinetically arrested inhomogeneous magnetic glass glassy (MG) state. We also studied the relationship between exchange bias and the frozen fraction of AST into the MST matrix.

2. Experimental details

2.1 Synthesis of melt-spun ribbon samples.

A bulk button shaped ingot was fabricated through arc melting under a highly pure argon atmosphere from high pure metallic elements (> 99.9 %). The ingot was further annealed at 1173 K for 24 hours in a sealed quartz tube under Ar atmosphere and followed by water quenching. From this sample, melt spun ribbons were obtained in a highly pure argon environment using a home-made single roller melt spinner system at a rotating speed of the copper wheel of 15 $m \cdot s^{-1}$. As-solidified ribbons were further sealed in a quartz ampoule that was thermally annealed at 1173 K for 24 hours and water quenched.

2.2 Structural, microstructural, thermal and magnetic characterization.

The critical temperatures of starting and finishing reverse and direct martensitic transformation of ribbons, hereafter referred to as A_S, A_f, M_S, and M_f, respectively, were determined by simple extrapolation from the differential scanning calorimetric (DSC) curves measured at heating/cooling rate of 5 $K \cdot min^{-1}$ in a TA model Q100 DSC system. The crystal structures of ribbons were examined with an X-ray diffractometer (XRD, Rigaku, Smartlab) with a 9 kW rotating anode using Cu-$K\alpha$ radiation. The measured temperatures for the XRD pattern of austenite and martensite were 298 and 253 K, respectively. The “step” mode was used with a

scanning step of 0.02° (2θ). Microstructural examinations and crystallographic orientation investigations were performed in a field emission gun scanning electron microscope (SEM, Jeol JSM 6500 F) with an EBSD acquisition camera and the Aztec online acquisition software package (Oxford Instruments). During the EBSD measurements, the "beam-control" mode was applied.

Magnetization measurements were carried out by vibrating sample magnetometry (VSM) in a Quantum Design PPMS® Dynacool®-9T platform. The magnetic field $\mu_o H$ was applied along the ribbon axis (i.e., the rolling direction) to minimize the effect of the internal demagnetizing field. The low-field (5 mT) and high-field (from 1 to 9 T) magnetization as a function of temperature $\sigma(T)$ curves were measured between 10 and 400 K. First, the sample was cooled from room temperature under zero applied magnetic field (ZFC process) to 10 K (the initial measuring temperature); then, the magnetic field is applied and the magnetization is measured while increasing the temperature up to 350 K; once the last point is measured, the sample is cooled back to the lowest temperature keeping the static field (FC process); finally, the magnetization was measured again by increasing the temperature (FH process). As the non-equilibrium field-cooled state at a given T is affected by the temperature-sweeping rate [18], in all the experiments this parameter was set at 1.0 K·min^{-1}. Accordingly, this criterion was not only followed to record $\sigma(T)$ curves, but also to reach any temperature at which a magnetization measurement versus field or time is performed or initiated.

3. Results and discussions

3.1 Structural and microstructural properties. Martensitic transition temperatures.

Fig. 1(a) shows the heating/cooling DSC scans along with the low-field (5 mT) ZFC, FC and FH $\sigma(T)$ curves (referred to as $\sigma(T)^{5mT}$). As stated before, from these curves we estimated the starting and finishing temperatures of the direct and reverse martensitic transformation. The values determined from the DSC [$\sigma(T)^{5mT}$] curves were: M_S= 277 (266) K, M_f= 253 (259) K, A_S=

287 (289) K and A_f = 306 (296) K. The Curie temperature of austenite, T_C^A = 400 K, was determined from the small step observed at the same temperature in the heating and cooling pathways of the DSC curves. From the DSC data, we estimated a transformation entropy change ΔS associated to the structural transition of 14.2 J kg^{-1} K^{-1}.

Fig. 1(b) shows the X-ray diffraction patterns of ribbon measured at its austenitic (298 K) and martensitic (253 K) state, respectively. It is seen that, in agreement with DSC and $\sigma(T)^{5mT\ cooling}$ curves, the ribbon samples are in a single austenitic state at room temperature. The observation of superlattice reflections $(111)_A$ and $(113)_A$ of austenite, representing the ordering degree of the constituent elements, suggests that the austenite has a highly ordered cubic $L2_1$-type crystal structure (space group *Fm-3m*), as inserted in the upper part of Fig. 1(b), rather than B2-type (space group *Pm-3m*) crystal structure [34]. The lattice parameter was determined to be 5.9818(5) Å. For the martensite phase, the appearance of satellite reflection $(\bar{1}\bar{2}1\bar{1})_M$ indicates that it has a modulated crystal structure [35]. Determinations show that the martensite of the studied ribbons has a monoclinic incommensurate 6M modulated martensite (superspace group I2/m(α0γ)00 [35]) with modulation wave vector $\boldsymbol{q}$= 0.3194(5)$\boldsymbol{c}^*$, which can be approximated by a three-fold layered superstructure model (as illustrated in the bottom part of Fig. 1(b)) in the three dimensional space. The similar crystal structures were also observed in the martensites of ternary Mn-rich Ni-Mn-In alloys [36]. The lattice parameters determined were a= 4.4064(8) Å, b= 5.5731(1) Å, c= 4.3344(6) Å and β= 93.943(1)°.

Fig. 2(a) and (b) displays SEM images of the free surface (BSE mode) and the fractured cross-section (SEI mode) of ribbon, respectively. It is seen that the microstructure consists of well-formed columnar grains growing along the entire ribbon thickness. The grain size of austenite is about 100 μm. Note that the cross-sectional microstructure of the studied ribbons differs from the one typically observed in as-solidified ones in which a thin layer of small equiaxed grains appear

in the surface in contact with the rotating copper wheel [37]. The absence of such a thin layer is attributed to the long thermal annealed performed (1173 K during 24 hours), which lead to the preferential grain growth of the dominant columnar in shape grains during annealing process. In addition, a very limited amount of martensite plates appear in some austenite grains. A characteristic orientation map appears in Fig. 2(c). It is seen that the *habit planes* between austenite and martensite are bordered by a single martensite variant.

3.2 Kinetic arrest of martensitic transformation.

The temperature dependencies of the magnetization $\sigma(T)$ under different applied static magnetic fields, ranging from 5 mT to 9 T, are shown in Fig. 3(a). As previously stated, the atypical behavior observed in the graphs, which reveals the occurrence of kinetic arrest of the martensitic transformation, is the magnetization difference between the ZFC and FC (or FH) pathways in the martensitic existence region (referred to as $\Delta\sigma^{FC\text{-}ZFC}$). Figs. 3(b) and (c) zoom into such difference for the $\sigma(T)$ curves measured at 5 and 7 T that reflect incomplete and complete arrest, respectively. The magnetic field dependence of the starting and finishing temperatures of the reverse and direct martensitic transformation, determined by simple extrapolation from the $\sigma(T)$ curves, and thermal hysteresis of the transformation ΔT_{hys}, determined as $\Delta T_{hys} = A_f - M_S$, are given in Fig. 3(d). Notice that A_S and A_f are plotted up to 7 T, while M_S and M_f are not given at this magnetic field value owing to the complete arrest of martensitic transformation on cooling. The expected decrease of the characteristic temperatures of both the reverse and direct martensitic transformation with the increase of the applied magnetic field is accompanied by the increase in ΔT_{hys}; the rate of change of A_S and A_f with applied field for the studied ribbons is about -9.6 KT^{-1}, while M_S and M_f decreased at a much faster rate of -17.8 KT^{-1} (almost double).

The metastable character of the magnetically inhomogeneous field-cooled two-phase state attained under a magnetic field of 5 T was characterized by means of different magnetization experiments designed to show the effects of energy fluctuations introduced, either by cycling the magnetic field or the temperature, in the martensitic existence temperature region; for the sake of comparison, similar experiments were conducted for the fully arrested state that is obtained at 7 T. These experiments will demonstrate that in both cases the system tends to the ZFC equilibrium state.

In the first test, thermal energy fluctuations were introduced through successive thermal cycling starting from a temperature of 10 K in both FC and ZFC states. In the former case the sample follows the FC regimen from 400 K to 10 K under a static magnetic field either of 5 or 7 T. Then the temperature is increased from 10 K to successively increasing maximum temperatures T_{max} of 50 K, 90 K, and 120 K; after the sample reaches the respective $T_{\max}$ temperature is decreased to 10 K. Along these increasing and decreasing temperature paths, the magnetic moment as a function of temperature is continuously measured. The $\sigma(T)^{5T}$ and $\sigma(T)^{7T}$ curves measured following this procedure are plotted in Figures 4(a) and (b) where the short vertical bars indicate the selected $T_{\max}$ values. The metastable character of the FC state is manifested by the magnetization decrement after successive temperature cycling since the thermal fluctuations gradually transform a small fraction of AST into MST, indicating that the system tends to the ZFC equilibrium state [3, 8]. On a second test, we started with the sample in ZFC state and followed the same thermal cycling procedure. As shown in Figures 4(a) and (b) that thermal energy fluctuations gradually increase the magnetization after each cycle. It is well known that in both martensite and austenite phases antiferromagnetic (AFM) and FM coupling between Mn magnetic moments coexist [38]. The introduction of thermal energy fluctuations leads to the metastable coupling of AFM moments with the applied magnetic field during the

cooling process originating the observed magnetization increase. Thus FC and ZFC methods lead to opposite behaviors underlying the metastable nature of the FC state.

In a second experiment, the sample is heated to 400 K, a strong magnetic field is applied and then the sample is field-cooled (FC) to different selected temperatures within the martensitic existence region that in the present case were 10, 50, 90 and 120 K; after reaching such temperatures the isothermal demagnetization curve $\sigma(\mu_o H)$ is measured by removing the magnetic field; this curve is usually referred as thermo-remanent (TR) demagnetization curve $\sigma(\mu_o H)^{TR}$ [1]. Once the field reaches zero value, subsequent magnetization/demagnetization $\sigma(\mu_o H)$ curves are measured by applying and removing the magnetic field. This experiment is useful to determine if the frozen AST will fully or partially transform into MST after removing and re-applying the magnetic field. In turns this is another way to prove the metastable nature of the FC inhomogeneous state. We performed this experiment for the same two applied magnetic fields, namely 5 and 7 T, this is for a partial and full kinetic arrest of the MT; the results obtained shown in Figs. 5(a) and (b), respectively. First note that at 10 K and 5 T $\sigma(\mu_o H)^{TR}$ and subsequent $\sigma(\mu_o H)$ curves overlap indicating that upon removal and re-applying the magnetic field no frozen AST transforms into MST. However, at 7 T the situation is different; in this case, a magnetization difference between $\sigma(\mu_o H)^{TR}$ and subsequent $\sigma(\mu_o H)$ curves is observed indicating that a fraction of AST has been transformed into MST. Vertical double arrows in Fig. 5 denote this irreversible magnetization change $\Delta\sigma^{irrev}$. As this difference results from the metastable nature of the FC inhomogeneous state it has the same origin than the splitting between ZFC and FC $\sigma(T)$ curves. Note that for both applied magnetic fields studied $\Delta\sigma(\mu_o H)^{irrev}$ increases with the temperature increase.

It has been pointed out that the dynamical behavior of this arrested non-equilibrium magnetic state, or magnetic glassy state, is very similar to those of structural glasses [32]. The relaxation of

magnetization in the FC kinetically arrested state is another phenomenon that characterizes the metastable nature of the magnetic glassy state [33]. For this state, the normalized magnetization as a function of time $\sigma/\sigma_o(t)$ at a fixed magnetic field value follows a Kohlrausch–Williams–Watts (KWW) stretched exponential function $\Phi \propto \exp[-(t/\tau)^{\beta}]$, where τ is a characteristic relaxation time and β a shape parameter [1]. β accounts for the number of intermediate states through which the system evolves and for different magnetic disordered systems its value lies between 0 and 1 [29, 39]. In order to check that our system follows this behavior and the validity of this model, in a third experiment we measured $\sigma/\sigma_o(t)$ curves at several temperatures in the martensitic existence region. Each of these temperature was reached following the same thermomagnetic protocol: cooling at a rate of 1 K·min^{-1} from 400 K under a static fields of 5 and 7 T applied at 400 K. The experimental relaxation curves measured at different temperatures in the FC pathway of the $\sigma(T)$ curve for static magnetic fields of 5 and 7 T are shown in Fig. 6(a) and (d), respectively (in all the cases σ was normalized to its zero-time value σ_o), whereas the fitting of the curves measured at 10 and 50 K for these two fields assuming a KWW stretched exponential function are shown in the bottom part as graphs (b) and (c), and (e) and (f), respectively. In all the cases the obtained values for the exponent β were around 0.95 indicating the weak metastable nature of the system under the strong magnetic fields applied.

The coexistence of AFM and FM interactions if the martensitic phase has been stated as the origin of the exchange bias (EB) effect observed in these Heusler alloys [40, 41]; this phenomenon typically occurs below a temperature that varies between 50 and 120 K depending on the alloy composition. For the observation of the EB, an external magnetic field must be applied at a temperature above the Néel temperature T_N of the AFM sublattice, and the sample must be field-cooled down to a temperature below; then, the magnetic field is removed and the FC hysteresis loop is recorded. Considering that the kinetic arrest retains a fraction of AST into the MST matrix reducing the volume fraction of MST, we have measured and compared the FC

hysteresis loops at 10 K under applied magnetic fields of 3, 5 and 7 T following two different thermomagnetic protocols referred hereafter as P1 and P2. They are as follows. In protocol P1 the sample is first heated up at zero-field to 400 K, cooled down to 130 K where a static magnetic field is applied and then cooled down to 10 K. At this temperature the FC hysteresis loop is measured. This is the typical thermomagnetic protocol followed to measure EB in these materials [40, 41]. In protocol P2 the sample is first heated up to 400 K where the magnetic field is applied and then cooled down to 10 K. At this temperature the FC hysteresis loop is measured. The results of these experiments are shown in Figure 7. The left- and right-hand columns of the figure show the FC hysteresis loops and a zoom into their low-field region, respectively, after following thermomagnetic protocols P1 and P2; the latter allows checking their shift along the $\mu_o H$-axis. The maximum saturation magnetization is consistent with the one derived from the respective curve $\sigma(T)$ curve; the splitting observed at 7 T for P2 agrees with the behavior denoted by the thermo-remanent curve. Fig. 7(g) shows the trend of the exchange bias ($\mu_o H_e$) and coercive ($\mu_o H_C$) fields. As expected, the sample shows $\mu_o H_e$ for thermal protocol P1 owing to the existence of MST; however, in the case of P2 the fraction of MST phase decreases when the field increases from 3 to 5 T becoming zero at 7 T, thus, in agreement $\mu_o H_e$ gradually decreases to reach zero.

4. Conclusions

The kinetic arrest effect of martensitic transformation observed in $Ni_{45}Co_5Mn_{36.8}In_{13.2\ 5}$ melt-spun ribbons was characterized by means of several magnetization experiments. In the ribbons fabricated austenite with a highly ordered cubic $L2_1$-type crystal structure transforms into a monoclinic martensite with incommensurate 6M modulated structure. With the increase of the magnetic field strength from 1 T, the volume fraction of $L2_1$-type austenite frozen into the martensitic matrix increases to a complete arrest of the structural transition for a magnetic field value equal or greater than 7 T. The metastable character of the non-equilibrium field-cooled

magnetic glass state was characterized by the decreasing trends of magnetization from a field-cooled arrested state when temperature or magnetic field fluctuations are introduced or during time evolution in the presence of a strong applied magnetic field. The latter follows a Kohlrausch–Williams–Watts (KWW) stretched exponential function with exponent β around 0.95 indicating the weak metastable nature of the system under strong magnetic fields. At last, a connection between the occurrence of exchange bias and the volume fraction of MST was found; in fact, the exchange bias field decreased with the decrease of the martensite fraction owing to the increasing fraction of arrested austenite.

Acknowledgments. This work was supported by Laboratorio Nacional de Investigaciones en Nanociencias y Nanotecnología (LINAN, IPICyT) and CONACYT, Mexico, under the grant CB-2012-01-183770. F.M. Lino-Zapata is grateful to CONACYT for supporting his Ph.D. studies (Grant No 332073). The authors also acknowledge the support received from the National Natural Science Foundation of China (Grants No. 51431005, 51571056, 51601033), the 863 Program of China (Grant No. 2015AA034101), and the 111 Project of China (Grant No. B07015).

References

[1] V.K. Sharma, M. Chattopadhyay, S.B. Roy, Phys. Rev. B. vol. **76** (2007) 140401.

[2] W. Ito, K. Ito, R.Y. Umetsu, R. Kainuma, K. Koyama, K. Watanabe, A. Fujita, K. Oikawa, K. Ishida, T. Kanomata, Appl. Phys. Lett. vol. **92** (2008) 021908.

[3] V.K. Sharma, M.K. Chattopadhyay, S.K. Nath, K.J. Sokhey, R. Kumar, P. Tiwari, S.B. Roy, J. Phys. Cond. Mater. vol. **22** (2010) 486007.

[4] W. Ito, R.Y. Umetsu, R. Kainuma, T. Kakeshita, K. Ishida, Scripta Mater. vol. **63** (2010) 73.

[5] Y. Lee, M. Todai, T. Okuyama, T. Fukuda, T. Kakeshita, R. Kainuma, Scripta Mater. vol. **64** (2011) 927.

[6] A.K. Nayak, K.G. Suresh, A.K. Nigam, J. Phys. Cond. Mater. vol. **23** (2011) 416004.

[7] R.Y. Umetsu, K. Ito, W. Ito, K. Koyama, T. Kanomata, K. Ishida, R. Kainuma, J. Alloys Compd. vol. **509** (2011) 1389.

[8] M.K. Chattopadhyay, K. Morrison, A. Dupas, V.K. Sharma, L.S. Sharath Chandra, L.F. Cohen, S.B. Roy, J. Appl. Phys. vol. **111** (2012) 053908.

[9] A. Lakhani, A. Banerjee, P. Chaddah, X. Chen, and R.V. Ramanujan, J. Phys. Cond. Mater. vol. **24** (2012) 386004.

[10] A. Banerjee, S. Dash, A. Lakhani, P. Chaddah, X. Chen, and R.V. Ramanujan, Solid State Commun. vol. **151** (2011) 971.

[11] F. Chen, Y.X. Tong, Y.J. Huang, B. Tian, L. Li, Y.F. Zheng, Intermetallics vol. **36** (2013) 81.

[12] D.M. Raj Kumar, N.V. Raman Rao, S. Esakki Muthu, S. Arumugan, M. Manivel Raja, K.G. Suresh, J. Def. Sci. vol. **66** (2016) 403.

[13] F.M. Lino-Zapata, J.L. Sánchez Llamazares, D. Ríos-Jara, A.G. Lara-Rodríguez, T. García-Fernández, Mater. Res. Soc. Symp. Proc. vol. **1485** (2013) 149.

[14] J.L. Sánchez Llamazares, B. Hernando, J.J. Suñol, C. García, C.A. Ross, J. Appl. Phys. vol.

107 (2010) 09A956.

[15] X. Xu, W. Ito, R.Y. Umetsu, K. Koyama, R. Kainuma, K. Ishida, Mater. Trans. vol. **51** (2010) 469.

[16] V. Siruguri, P.D. Babu, S.D. Kaushik, A. Biswas, S.K. Sarkar, M. Krishnan, P. Chaddah, J. Phys. Cond. Mater. vol. **25** (2013) 496011.

[17] M.A. Manekar, S. Chaudhary, M.K. Chattopadhyay, K.J. Singh, S.B. Roy, P. Chaddah, Phys. Rev. B. vol. **64** (2001) 104416.

[18] S.B. Roy, G. Perkins, M. Chattopadhyay, A. Nigam, K. Sokhey, P. Chaddah, A. Caplin, L. Cohen, Phys. Rev. Lett. vol. **92** (2004) 147203.

[19] M. Chattopadhyay, S. Roy, P. Chaddah, Phys. Rev. B. vol. **72** (2005) 180401.

[20] K. Kumar, A. Pramanik, A. Banerjee, P. Chaddah, S. Roy, S. Park, C. Zhang, S.W. Cheong, Phys. Rev. B. vol. **73** (2006) 184435.

[21] R. Rawat, P. Chaddah, P. Bag, P.D. Babu, V. Siruguri, J. Phys. Cond.. Mater. vol. **25** (2013) 066011.

[22] S.B. Roy, M.K. Chattopadhyay, P. Chaddah, J.D. Moore, G.K. Perkins, L.F. Cohen, K.A. Gschneidner, V.K. Pecharsky, Phys. Rev. B. vol. **74** (2006) 012403.

[23] S.B. Roy, M.K. Chattopadhyay, Europhys. Lett. vol. **79** (2007) 47007

[24] X. Xu, W. Ito, M. Tokunaga, R.Y. Umetsu, R. Kainuma, K. Ishida, Mater. Trans. vol. **51** (2010) 1357.

[25] A.K. Nayak, M. Nicklas, C. Shekhar, C. Felser, J. Appl. Phys. vol. **113** (2013) 17E308.

[26] Ö. Çakır, M. Acet, M. Farle, E. Dias, K. Priolkar, J. Magn. Magn. Mater. vol. **390** (2015) 96.

[27] R. Rawat, K. Mukherjee, K. Kumar, A. Banerjee, P. Chaddah, J. Phys. Cond. Mater. vol. **19** (2007) 256211.

[28] A. Banerjee, A.K. Pramanik, Kranti Kumar, P. Chaddah, J. Phys. Cond. Mater. vol. **18**

(2006) L605.

[29] S. Chatterjee, S. Giri, S. Majumdar, J. Phys. Cond. Mater. vol. **24** (2012) 366001.

[30] S.B. Roy, J. Phys. Cond. Mater. vol. **25** (2013) 183201.

[31] J. Kurchan, Nature vol. **433** (2005) 222.

[32] P.G. Debenedetti, F.H. Stillinger, Nature vol. **410** (2001) 259.

[33] P.W. Anderson, Science vol. **267** (1995) 1615.

[34] H.L. Yan, C.Y. Zhang, Y.D. Zhang, X.L. Wang, C. Esling, X. Zhao, L. Zuo, J. Appl. Cryst. vol. **49** (2016) 1585.

[35] S. van Smaalen, Incommensurate Crystallography, Oxford University Press, Oxford, 2007.

[36] H.L. Yan, Y.D. Zhang, N. Nu, A. Senyshyn, H.-G. Brokmeier, C. Esling, X. Zhao, L. Zuo, Acta Mater. vol. **88** (2015) 375.

[37] Aris Quintana-Nedelcos, J.L. Sánchez Llamazares, D. Ríos-Jara, A.G. Lara-Rodríguez, T. García-Fernández, Phys. Status Solidi A vol. 210 (2013) 2159-2165.

[38] T. Krenke, M. Acet, E.F. Wassermann, X. Moya, L. Mañosa, A. Planes, Phys. Rev. B. vol. **73** (2006) 174413.

[39] X. Du, G. Li, E.Y. Andrei, M. Greenblatt, P. Shuk, Nat. Phys. vol. **3** (2007) 111.

[40] B. M. Wang, Y. Liu, L. Wang, S. L. Huang, Y. Zhao, Y. Yang, H. Zhang, J. Appl. Phys. vol. **104** (2008) 043916.

[41] A. Kumar, M. Khan, B.R. Gautam, S. Stadler, I. Dubenko N. Ali, J. Magn. Magn. Mater. vol. **321** (2008) 963.

FIGURE CAPTIONS

Fig. 1. (a) ZFC, FC and FH $\sigma(T)$ curves at 5 mT and DSC scans in the temperature range of the structural transition region (black line). (b) X-ray diffraction patterns of austenite (top) and martensite (bottom) of ribbons measured at 298 K and 253 K, respectively.

Fig. 2. SEM images of the free surface (a) and the fractured cross-section (b) of ribbons and orientation map of austenite and martensite where the two phases are colored according to their crystallographic orientations (c).

Fig. 3. (a) ZFC, FC and FH $\sigma(T)$ curves measured under various static magnetic fields from 5 mT to 9 T. (b) and (c) zoom into the $\sigma(T)$ curves in the martensitic region at 5 and 7 T, respectively, to point on the magnetization difference $\Delta\sigma^{FC\text{-}ZFC}$ between the ZFC and FC pathways of the curves. (d) Magnetic field dependence of the starting and finishing temperatures and thermal hysteresis of the transformation ΔT_{hys} (determined as $\Delta T_{hys} = A_f - M_S$) for the reverse and direct martensitic transformation.

Fig. 4. Effect of the successive thermal cycling between 10 K and T_{max}, for T_{max} = 50 K, 90 K, and 120 K, on the ZFC and FC $\sigma(T)$ curve at 5 T (a) and 7 T (b).

Fig. 5. Demagnetization thermo-remanent curve $\sigma(\mu_o H)^{TR}$ followed by the subsequent field-up and field-down $\sigma(\mu_o H)$ curves measured at different temperatures in the martensitic existence region i.e., below 120 K); single and double arrows indicated the sweeping field direction. The irreversible magnetization change $\Delta\sigma(\mu_o H)^{irrev}$ at 50 K is indicated by the vertical double arrow.

Fig. 6. Normalized magnetization σ/σ_o versus time plots at several temperatures in the martensitic existence region measured under static field of 5 T (a) and 7 T (d). The experimental $\sigma/\sigma_o(t)$ curves measured at 10 and 50 K and their fitting (solid red line) to a KWW stretched exponential function are given in (b) and (c) for 5 T, and in (e) and (f) for 7 T.

Fig. 7. Left-hand side top column: FC hysteresis loops at 10 K measured following thermal protocols P1 and P2 under applied magnetic fields of 3 (a), 5 (b) and 7 T (c). Right-hand side top column: zoom into the low-field region of the FC hysteresis loops measured following thermal protocols P1 and P2 under applied magnetic fields of measured at 3 (d), 5 (e) and 7 T (f) following thermal protocols P1 and P2. (g) Coercive field $\mu_o H_C$ and exchange bias $\mu_o H_e$ fields as a function of the applied magnetic field.

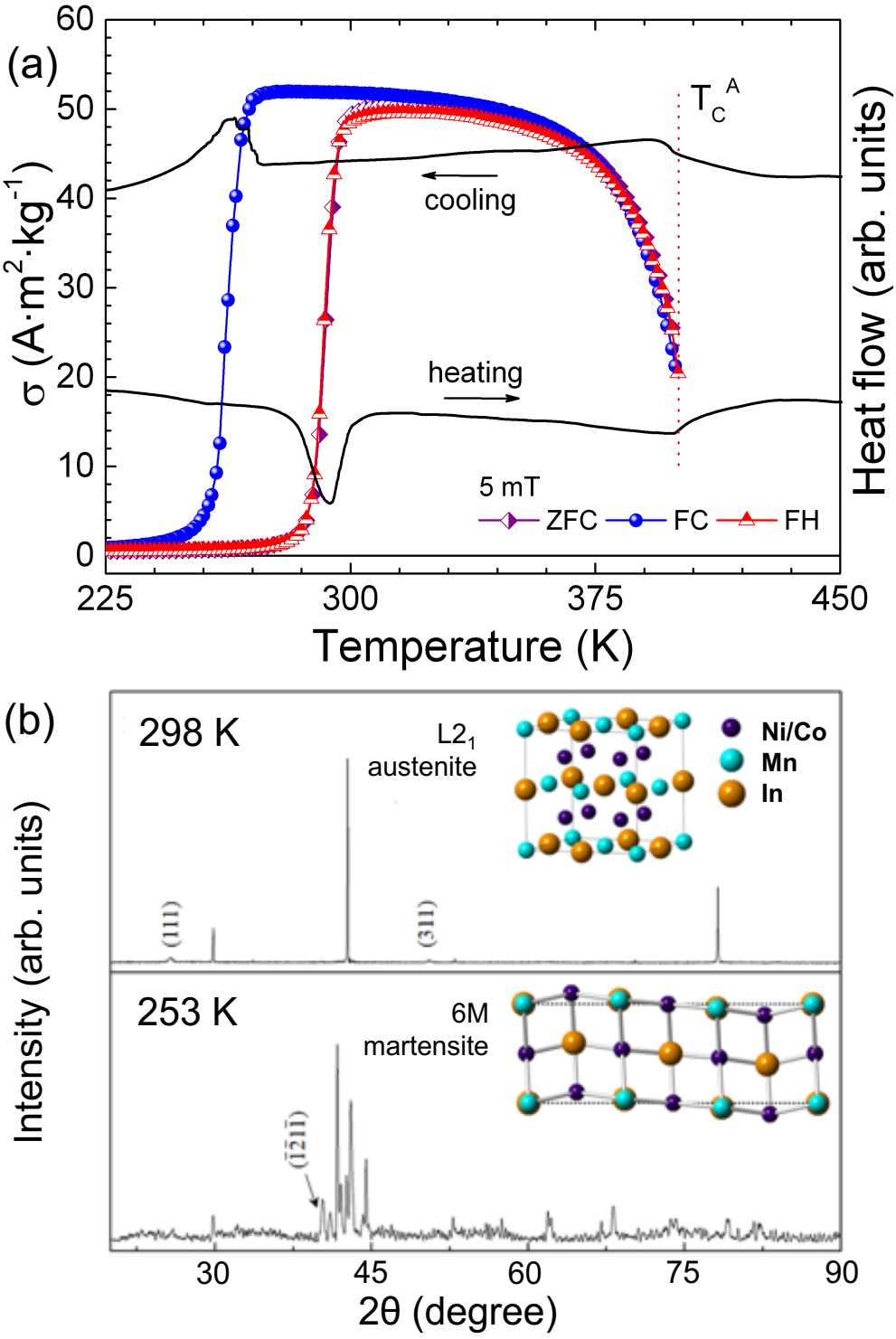

Fig. 1. (a) ZFC, FC and FH $\sigma(T)$ curves at 5 mT and DSC scans in the temperature range of the structural transition region (black line). (b) X-ray diffraction patterns of austenite (top) and martensite (bottom) of ribbons measured at 298 K and 253 K, respectively..

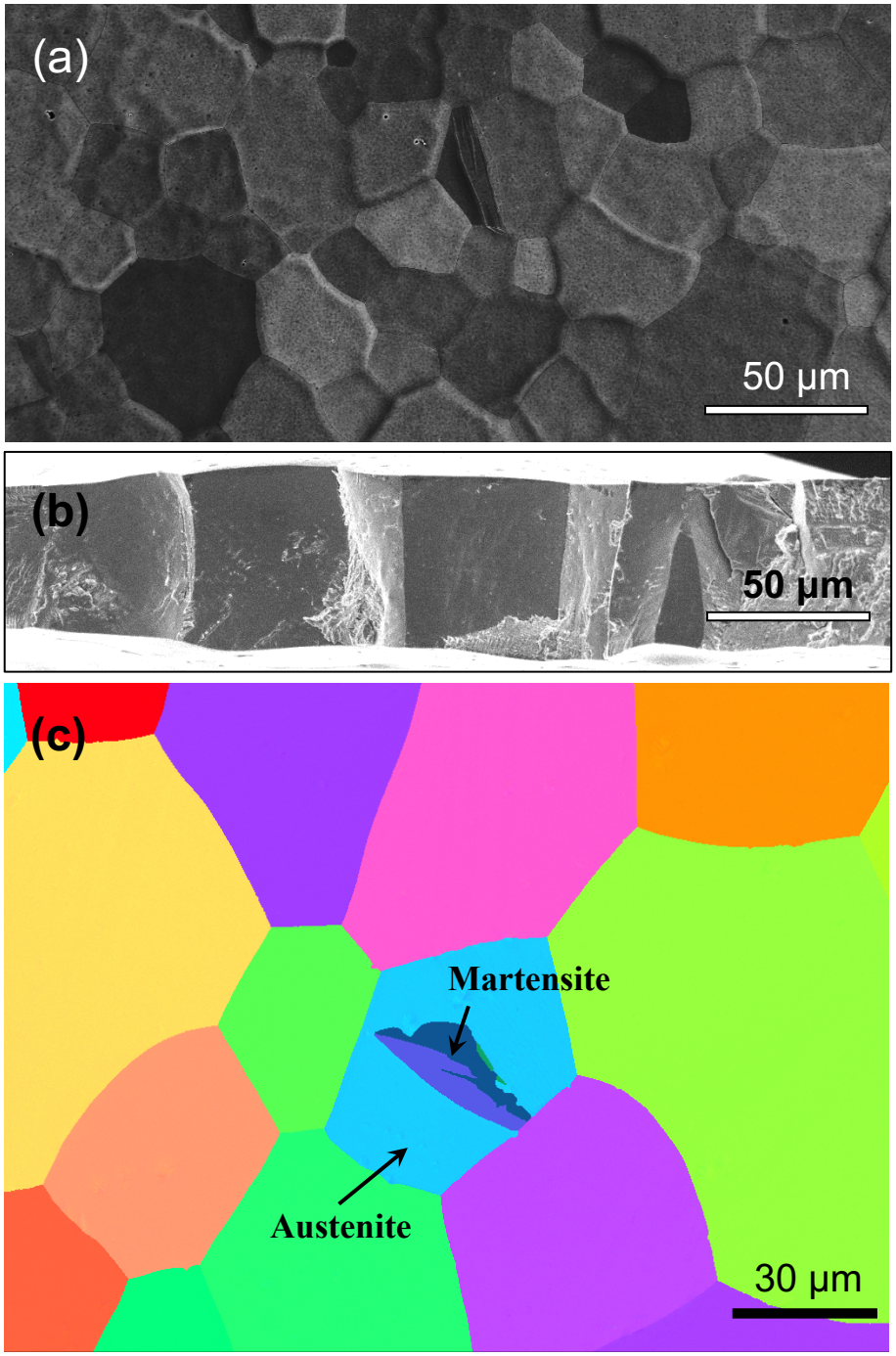

Fig. 2. SEM images of the free surface (a) and the fractured cross-section (b) of ribbons and orientation map of austenite and martensite where the two phases are colored according to their crystallographic orientations (c).

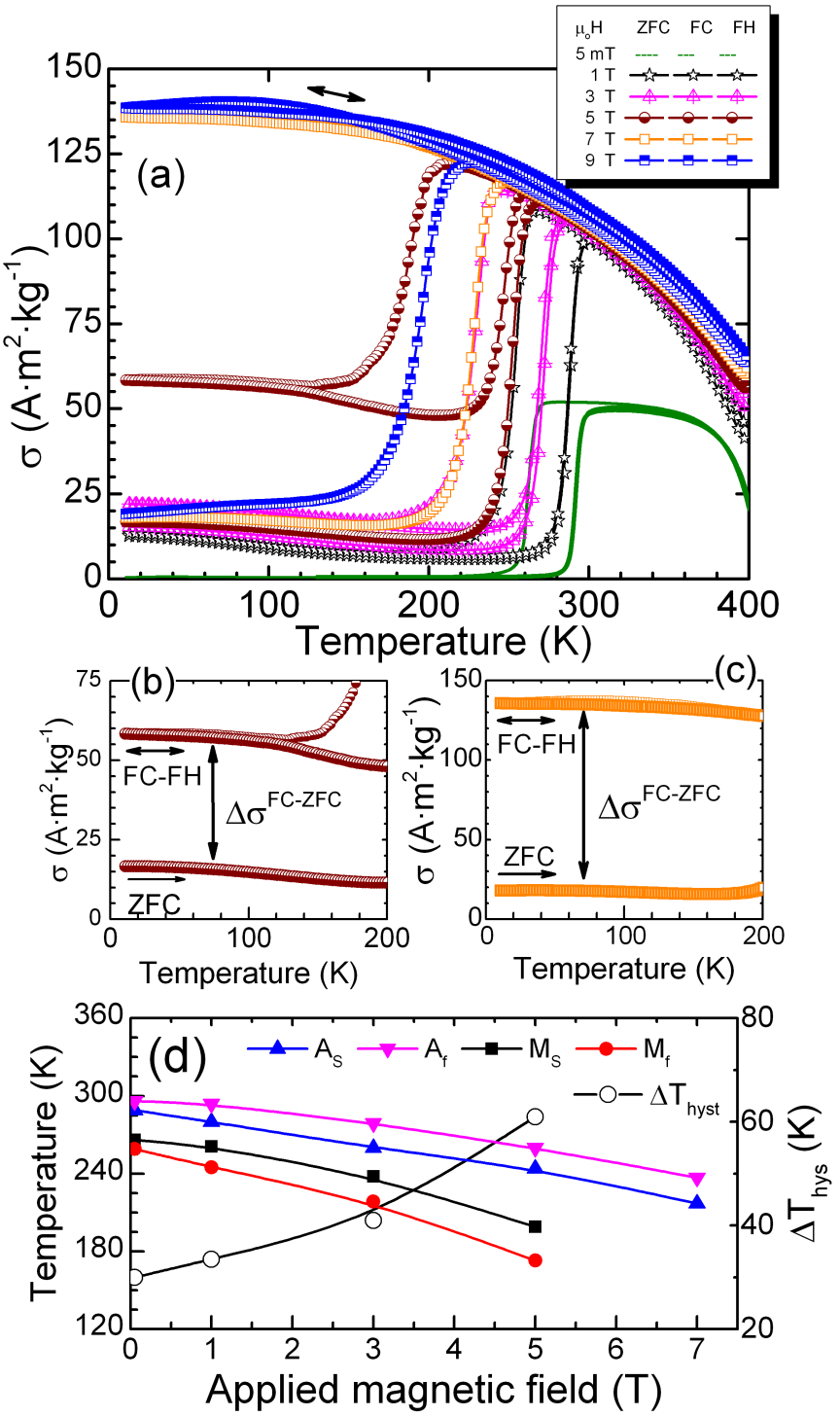

Fig. 3. (a) ZFC, FC and FH $\sigma(T)$ curves measured under various static magnetic fields from 5 mT to 9 T. (b) and (c) zoom into the $\sigma(T)$ curves in the martensitic region at 5 and 7 T, respectively, to point on the magnetization difference $\Delta\sigma^{FC\text{-}ZFC}$ between the ZFC and FC pathways of the curves. (d) Magnetic field dependence of the starting and finishing temperatures and thermal hysteresis of the transformation ΔT_{hys} (determined as $\Delta T_{hys} = A_f - M_S$) for the reverse and direct martensitic transformation.

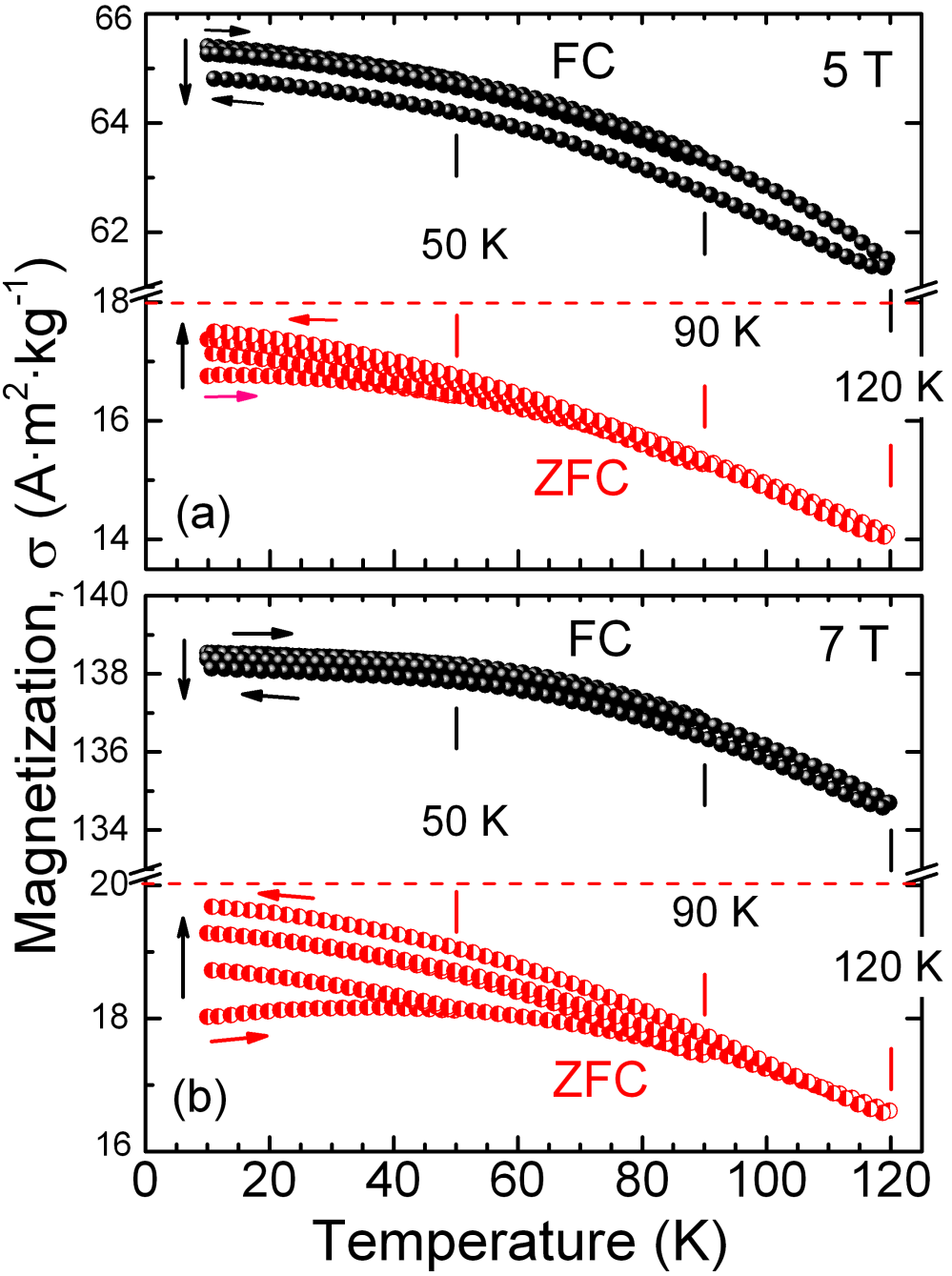

Fig. 4. Effect of the successive thermal cycling between 10 K and T_{max}, for T_{max} = 50 K, 90 K, and 120 K, on the ZFC and FC $\sigma(T)$ curve at 5 T (a) and 7 T (b).

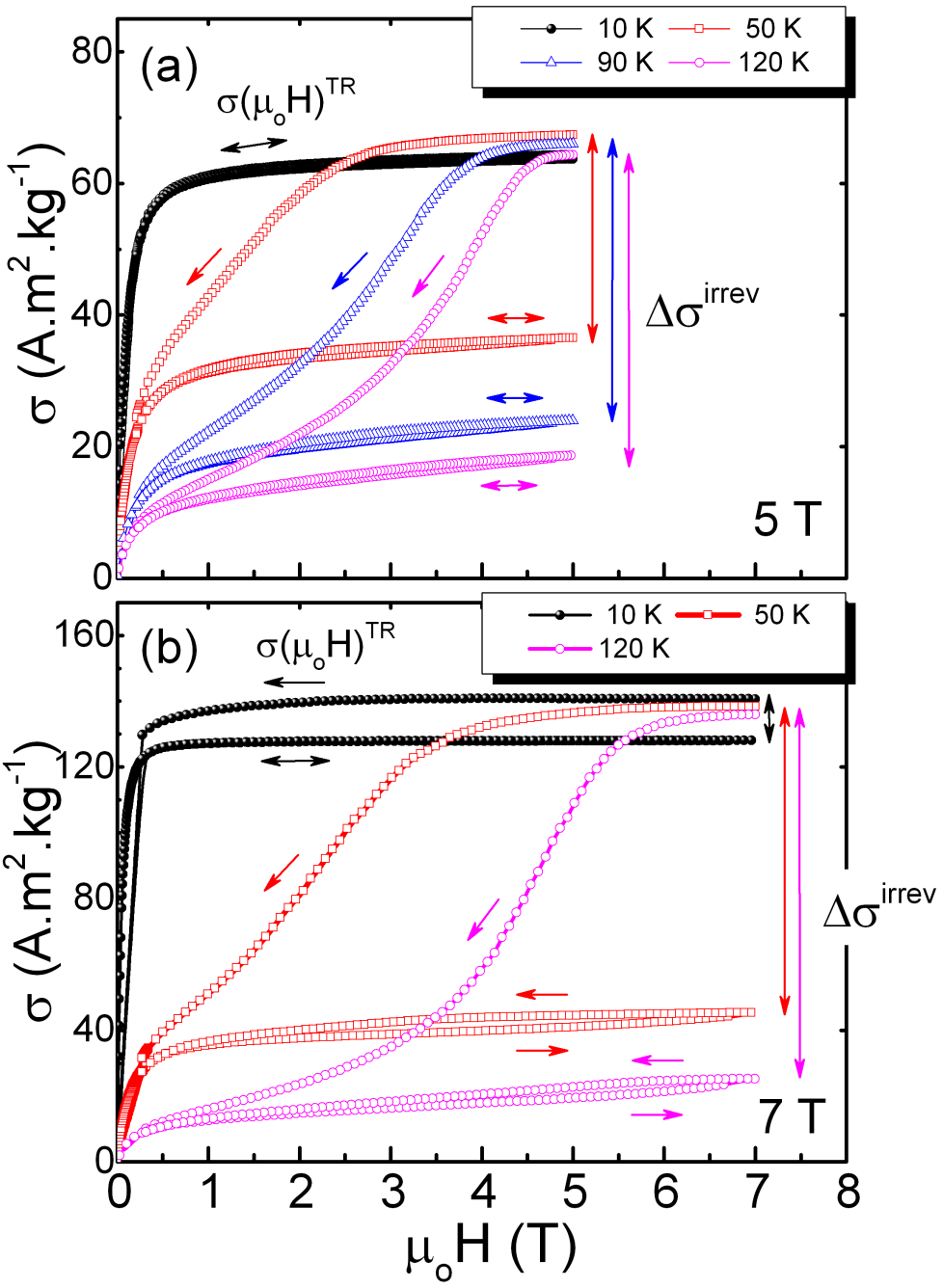

Fig. 5. Demagnetization thermo-remanent curve $\sigma(\mu_o H)^{TR}$ followed by the subsequent field-up and field-down $\sigma(\mu_o H)$ curves measured at different temperatures in the martensitic existence region i.e., below 120 K); single and double arrows indicated the sweeping field direction. The irreversible magnetization change $\Delta\sigma(\mu_o H)^{irrev}$ at 50 K is indicated by the vertical double arrow.

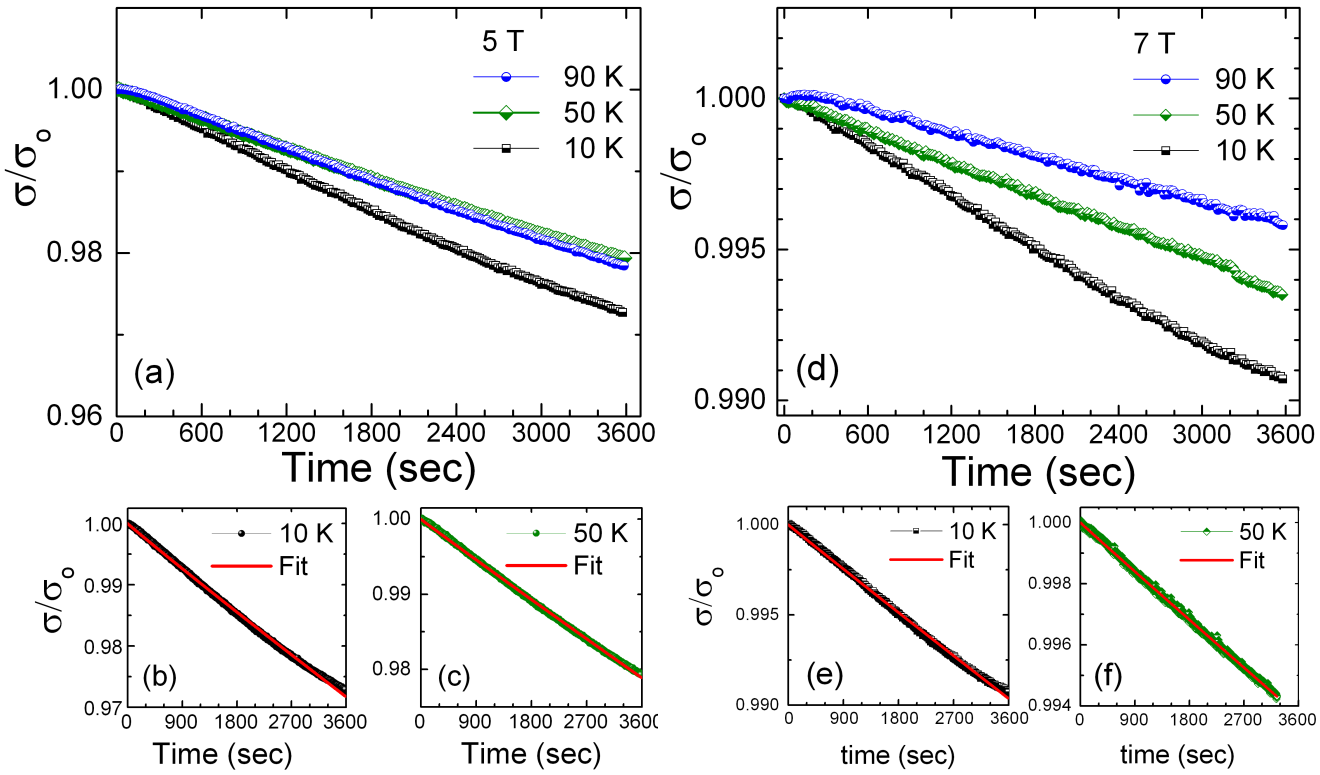

Fig. 6. Normalized magnetization σ/σ_o versus time plots at several temperatures in the martensitic existence region measured under static field of 5 T (a) and 7 T (d). The experimental $\sigma/\sigma_o(t)$ curves measured at 10 and 50 K and their fitting (solid red line) to a KWW stretched exponential function are given in (b) and (c) for 5 T, and in (e) and (f) for 7 T.

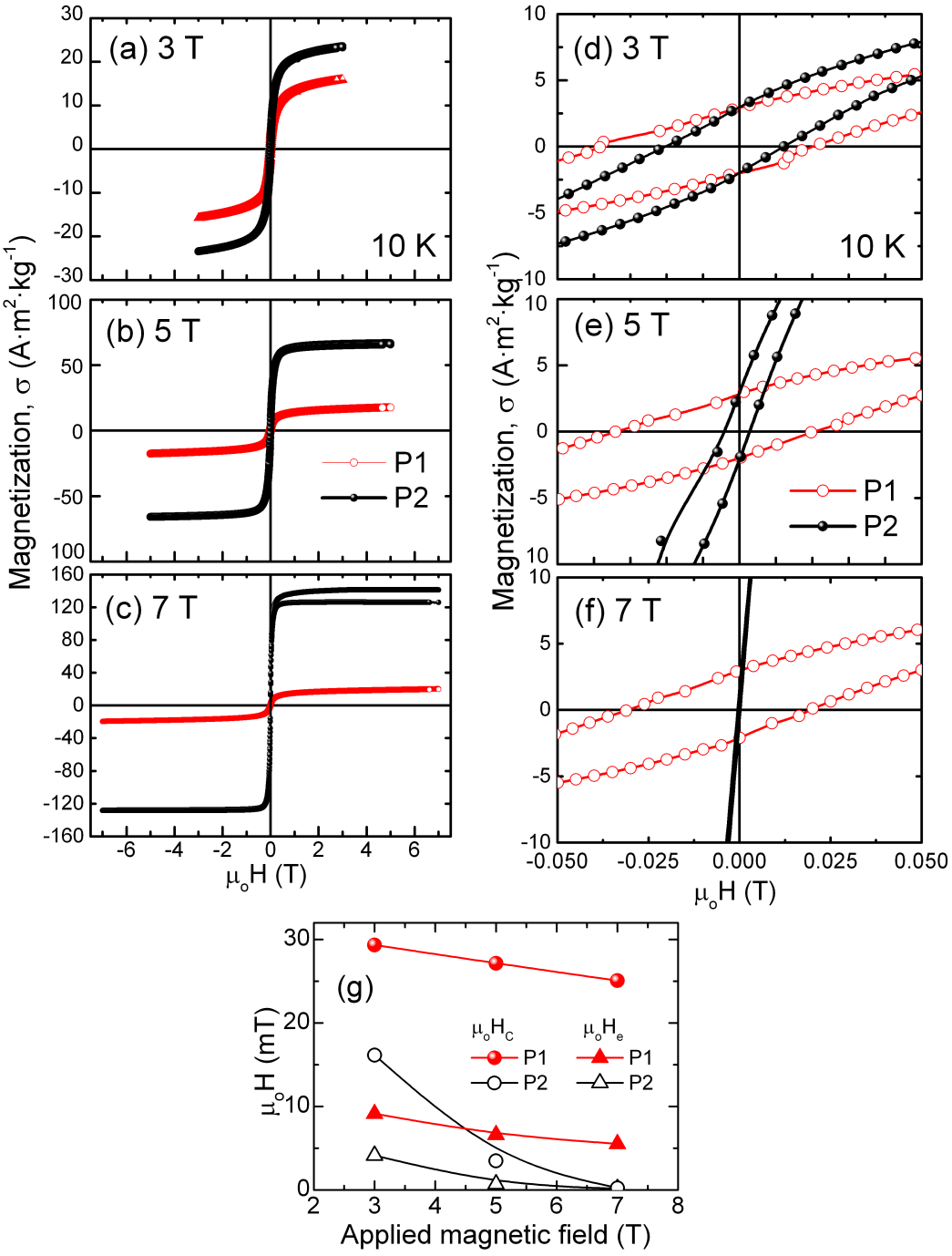

Fig. 7. Left-hand side top column: FC hysteresis loops at 10 K measured following thermal protocols P1 and P2 under applied magnetic fields of 3 (a), 5 (b) and 7 T (c). Right-hand side top column: zoom into the low-field region of the FC hysteresis loops measured following thermal protocols P1 and P2 under applied magnetic fields of measured at 3 (d), 5 (e) and 7 T (f) following thermal protocols P1 and P2. (g) Coercive field $\mu_o H_C$ and exchange bias $\mu_o H_e$ fields as a function of the applied magnetic field.